

Guideline for a Simplified Differential-Mode EMI Filter Design

Klaus Raggl, *Student Member, IEEE*, Thomas Nussbaumer, *Member, IEEE*, and Johann W. Kolar, *Senior Member, IEEE*

Abstract—The design of electromagnetic interference (EMI) input filters, needed for switched power converters to fulfill the regulatory standards, is typically associated with high development effort. This paper presents a guideline for a simplified differential-mode (DM) filter design. First, a procedure to estimate the required filter attenuation based on the total input rms current using only a few equations is given. Second, a volume optimization of the needed DM filter based on the previously calculated filter attenuation and volumetric component parameters is introduced. It is shown that a minimal volume can be found for a certain optimal number of filter stages. The considerations are exemplified for two single-phase power factor correction converters operated in continuous and discontinuous conduction modes, respectively. Finally, EMI measurements done with a 300-W power converter prototype prove the proposed filter design method.

Index Terms—Design guideline, electromagnetic compatibility, electromagnetic interference (EMI), noise estimation, volume optimization.

I. INTRODUCTION

SWITCHED POWER supplies with power factor correction (PFC) have become very popular in the past in order to increase the power density and to fulfill low-frequency harmonic standards [1]. However, due to the high-frequency switched current, high-frequency conducted emissions will also appear. To protect the mains from these emissions and comply with the high-frequency harmonic standards [2], electromagnetic interference (EMI) filters are imperatively needed.

Since the differential-mode (DM) noise typically leads to the major filter part and is therefore mainly determining the power density of the converter, the focus of this paper will be laid only on DM noise emissions.

In the past, high effort has been carried out in order to estimate the emitted DM EMI noise [3], [4], reduce the emitted noise by specific circuit designs [5]–[8], or design a proper filter to attenuate the noise emissions [9]–[13] prior to an experimental testing in order to achieve an optimal filter and converter design and avoid trial and error in the design process. The focus of this paper will be to estimate the appearing noise emissions, derive the needed filter requirements, and design a

Manuscript received February 17, 2009; revised July 13, 2009. First published August 7, 2009; current version published February 10, 2010.

K. Raggl is with Hilti AG, 9494 Schaan, Liechtenstein (e-mail: klaus.raggl@hilti.com).

T. Nussbaumer is with Levitronix GmbH, 8005 Zurich, Switzerland.

J. W. Kolar is with the Power Electronic Systems Laboratory (PES), Swiss Federal Institute of Technology (ETH) Zurich, 8092 Zurich, Switzerland.

Color versions of one or more of the figures in this paper are available online at <http://ieeexplore.ieee.org>.

Digital Object Identifier 10.1109/TIE.2009.2028293

DM EMI filter with minimal volume in a simple straightforward procedure.

In this paper, a new simplified method to estimate the appearing noise voltage at a specific design frequency f_D will be presented. With the introduced method, a designer only has to simulate or calculate the converter input current. After a short explanation of the conventional DM filter design routine in Section II, a new method to estimate the expected attenuation by only using a few equations is given in Section III. Subsequently, a guideline for the selection of the filter component values which lead to a minimum volume filter is given in Section IV. Two examples for the filter design by calculation and simulation of the converter input current are presented in Section V. Final measurements, which prove the proposed design guideline, will be shown in Section VI.

II. CONVENTIONAL DM FILTER DESIGN APPROACH

The realization of an EMI filter to attenuate the DM noise emissions is shown in Fig. 1, together with a simplified circuit of the line impedance stabilization network (LISN), which is defined in the standards [2] in order to guarantee repeatable measurement results independently on the mains impedance. As for the used filter, n_f LC filter stages are used to attenuate the DM noise emissions sufficiently. The symmetrical arrangement of the filter inductors leads to an additional attenuation of the so-called mixed-mode noise emissions in combination with the DM capacitors [14], [15]. As shown in [16], realizing the n_f filter stages with the same inductance $L_1 = L_2 = \dots = L_{nf} = L$ and capacitor values $C_1 = C_2 = \dots = C_{nf} = C$ leads to a minimum volume design.

The filter component values are mainly depending on the required filter attenuation, which has to be provided by the EMI filter at a specific design frequency f_D . The calculation of this required attenuation Att_{req} is done in the following way [3]:

- 1) simulation or calculation of the converter input current;
- 2) calculation of the voltage $U_{LISN}(t)$;
- 3) transferring $U_{LISN}(t)$ into the frequency domain by Fourier analysis;
- 4) bandpass filtering of $U_{LISN}(f)$ with 9 kHz [2] around a sweep frequency f_{sweep} ;
- 5) transferring the bandpass-filtered voltage into the time domain by inverse Fourier analysis;
- 6) calculation of the quasi-peak (QP) noise voltage $U_{QP}(f_{sweep})$ at the sweep frequency f_{sweep} by a QP detection circuit being defined in [17];

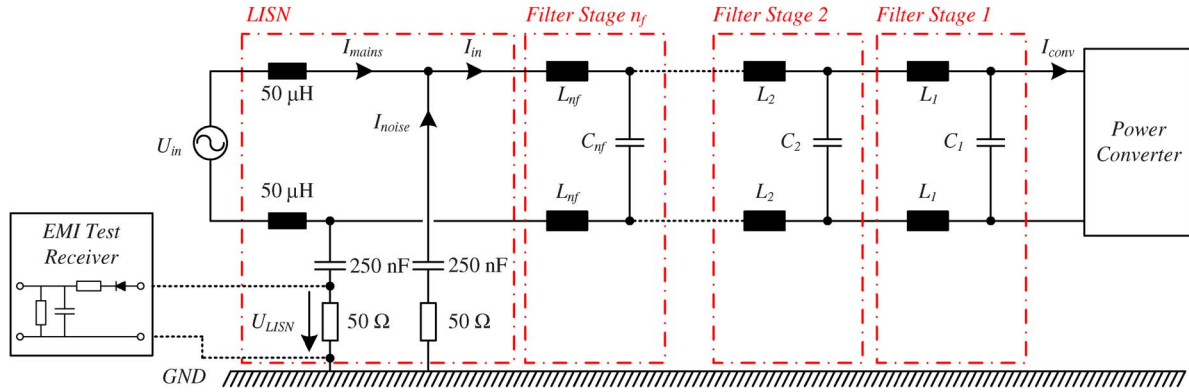


Fig. 1. Topology of a DM input filter with n_f filter stages and the simplified LISN together with the EMI test receiver.

- 7) lowpass filtering (with a time constant of 160 ms [17]) of the voltage in the time domain;
- 8) repeating steps 4) to 7) with f_{sweep} varying in the frequency range of 150 kHz–30 MHz;
- 9) comparing the noise voltage $U_{\text{QP}}(f)$ in the frequency range of 150 kHz–30 MHz with the limits given in [17]. The height of the first voltage peak appearing beyond 150 kHz leads to the required attenuation Att_{req} at the “design frequency” f_D (defined as a positive value)

$$Att_{\text{req}}(f_D) [\text{dB}] = U_{\text{QP}}(f_D) [\text{dB} \cdot \mu\text{V}] - Limit(f_D) [\text{dB} \cdot \mu\text{V}] + Margin [\text{dB}] \quad (1)$$

including a margin to accommodate parameter tolerances and drifts.

Now, a DM filter has to be applied, which, at least, delivers the required attenuation Att_{req} at the design frequency f_D in order to fulfill the standards.

The attenuation Att_{LC} of an LC filter with n_f filter stages and same component values for all filter stages is generally given by [3], [16]

$$Att_{\text{LC}}(f_D) = (2\pi \cdot f_D)^{2n_f} \cdot (2L)^{n_f} \cdot C^{n_f} \geq Att_{\text{req}}(f_D) \quad (2)$$

and has to be larger than the required attenuation Att_{req} as mentioned before.¹

One can see that this conventional EMI filter design leads to time-intensive and complex calculations, particularly concerning the calculation of the QP noise voltage. Therefore, a simplified design routine for DM filter design will be presented subsequently.

III. NOVEL SIMPLIFIED DM FILTER DESIGN APPROACH

The main idea of the new introduced method is shown in Fig. 2. It is based on the assumption that the total high-frequency *rms* noise current is an adequate measure for the estimation of the QP detection voltage at the EMI test receiver.

¹It has to be stated that, for very high switching frequencies ($f_S \geq 500$ kHz), the parasitics of L and C also have to be taken into account, which is not done here for the sake of simplicity.

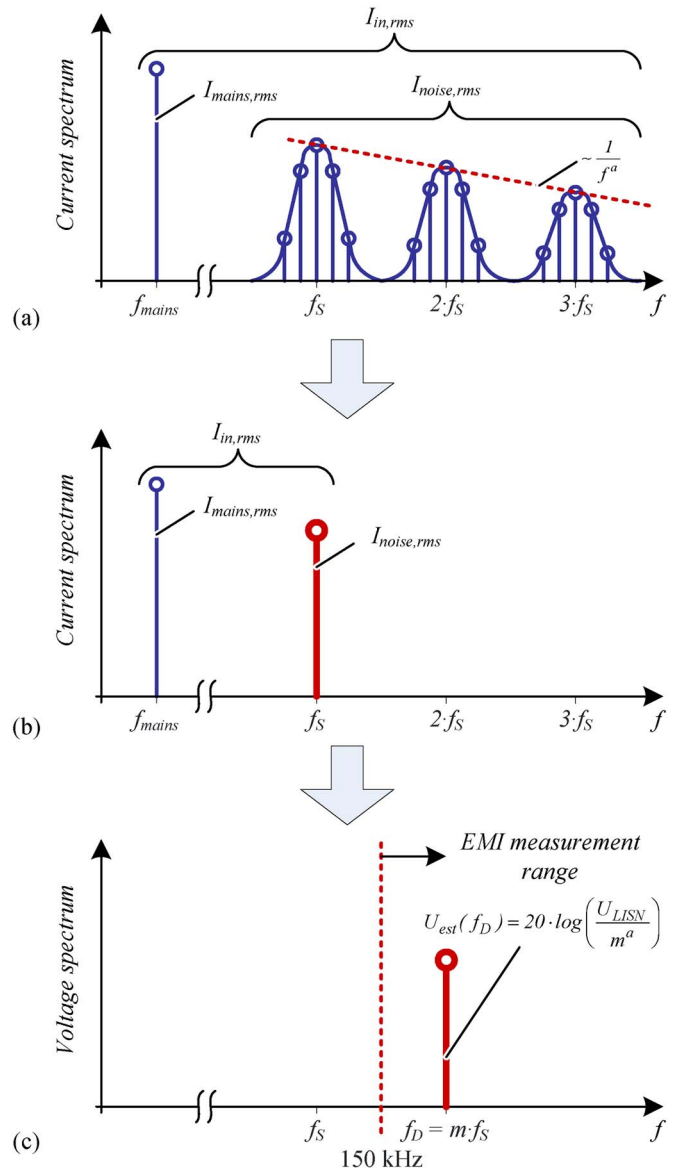
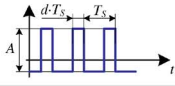
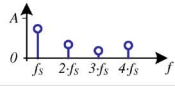
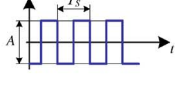
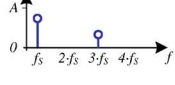
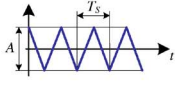
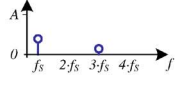
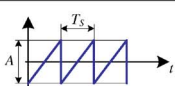
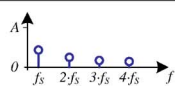


Fig. 2. Main idea of the noise estimation by (b) summing up all high-frequency current components in (a) to only one component at the switching frequency f_S and (c) calculating the estimated noise voltage at the design frequency f_D .

TABLE I
CALCULATION OF THE NOISE ESTIMATION ERROR

Time domain	Frequency domain	Amplitudes	Error $e = \frac{c_{tot,rms}}{ c_1,rms }$
(a) 		$ c_1 _{rms} = \frac{1}{\sqrt{2}} \cdot \frac{2A}{\pi} \cdot \sin(\pi \cdot d)$ $c_{tot,rms} = A \cdot \sqrt{d - d^2}$	$e_{d=0.1} = e_{d=0.9} = 2.16 = 6.7 \text{ dB}$ $e_{d=0.3} = e_{d=0.7} = 1.26 = 2 \text{ dB}$ $e_{d=0.5} = 1.11 = 0.9 \text{ dB}$
(b) 		$ c_1 _{rms} = \frac{1}{\sqrt{2}} \cdot \frac{2A}{\pi}$ $c_{tot,rms} = \frac{A}{2}$	$e = \frac{\pi}{2 \cdot \sqrt{2}} = 1.11 = 0.9 \text{ dB}$
(c) 		$ c_1 _{rms} = \frac{1}{\sqrt{2}} \cdot \frac{4A}{\pi^2}$ $c_{tot,rms} = \frac{A}{2 \cdot \sqrt{3}}$	$e = \frac{\pi^2}{4 \cdot \sqrt{6}} = 1.01 = 0.1 \text{ dB}$
(d) 		$ c_1 _{rms} = \frac{1}{\sqrt{2}} \cdot \frac{A}{\pi}$ $c_{tot,rms} = \frac{A}{2 \cdot \sqrt{3}}$	$e = \frac{\pi}{\sqrt{6}} = 1.28 = 2.2 \text{ dB}$

For the estimation, it is assumed that the total noise current $I_{noise,rms}$ [which consists of several harmonics at multiples of the switching frequency with according sidebands, cf. Fig. 2(a)] would appear as a single peak only at the switching frequency [cf. Fig. 2(b)]. This peak would then cause a noise voltage at the test receiver, which is very easy to calculate. Only, it has to be considered that, for switching frequencies below the EMI measurement range 150 kHz–30 MHz and/or for interleaved operation of parallel converters, the estimated voltage has to be adjusted adequately [cf. Fig. 2(c)], as will be shown in the following.

The estimation can be interpreted such that practically the whole noise energy is present in the first harmonic peak. In order to estimate the accuracy of this approximation, an analytical calculation is presented in Table I. Here, for several high-frequency input current waveforms,² namely, a pulse wave current (a) with the duty cycle d , a square wave current (b), and a triangular (c) and a sawtooth waveform (d), the magnitudes $|c_1|_{rms}$ of the first peaks appearing at the switching frequency $f_s = 1/T_s$ are compared with the total rms current $c_{tot,rms}$ (calculated in the time domain). The error, by assuming that the whole noise energy is present in the first appearing peak, can now be calculated by

$$e = \frac{c_{tot,rms}}{|c_1|_{rms}} \quad (3)$$

and is compiled in Table I, for all four waveforms. One can see that the errors for the signals (a)–(d) are in the range of 2 dB. Only for pulse-shaped waveforms with duty cycles $d \leq 0.3$ or $d \geq 0.7$, the error will be larger (i.e., 6.7 dB for $d = 0.1$). However, this error will be smaller in practice since the duty cycle is varying over one mains period. In this estimation, it is further assumed that the noise energy of eventual sidebands of the first harmonic is already included in the calculated value. In this case, the input signal of the QP detector is only given by a single sine wave, and the output signal would be

²It has to be noted that the fundamental input current frequency, which corresponds with the mains frequency, can be neglected for this consideration.

exactly the rms value of this signal [due to the gain of $1/\sqrt{2}$ (cf. [3])]. The validity of this assumption will vary from case to case, depending on the specific shape of the sidebands (due to different topologies and modulation schemes), but it will be quantitatively shown by simulations in Section V that, for typical waveforms, the error is in an acceptable range.

Concerning the calculation of the noise estimation, the total rms input current $I_{in,rms}$ is equal to the converter input current I_{conv} prior to the filter design (cf. Fig. 1) and can be derived by analytical calculation and/or circuit simulation (cf. Section V). This current can generally be separated into one part $I_{mains,rms}$, caused by the delivered power and appearing at the mains frequency f_{mains} , and a second part $I_{noise,rms}$ containing all high-frequency harmonics appearing at the switching frequency f_s [cf. Fig. 2(b)]. Consequently, the rms value of this total noise current can be written as

$$I_{noise,rms}^2 = I_{in,rms}^2 - I_{mains,rms}^2 \quad (4)$$

with $I_{mains,rms}$ depending on the delivered power P_{in} and the rms mains voltage $U_{in,rms}$

$$I_{mains,rms} = \frac{P_{in}}{U_{in,rms}} \cdot \cos \varphi \quad (5)$$

with φ being the phase difference between the input current I_{in} and the input voltage U_{in} , whereby φ is equal to zero in case of an ideal PFC.

Looking at Fig. 1, the high-frequency current $I_{noise,rms}$ is in a first simplification blocked completely by the LISN inductance and leads furthermore to the voltage drop U_{LISN} (the LISN capacitance acts as a short circuit for high frequencies). On the contrary, the low-frequency current $I_{mains,rms}$ will be blocked by the LISN capacitor, and thus, no voltage drop U_{LISN} will appear due to this current. Therefore, the appearing voltage U_{LISN} in the time domain can now be calculated easily as

$$U_{LISN} \approx 50 \Omega \cdot I_{noise,rms} \quad (6)$$

As for the design frequency, the first noise peak is appearing at the switching frequency f_s . As a result, the design frequency

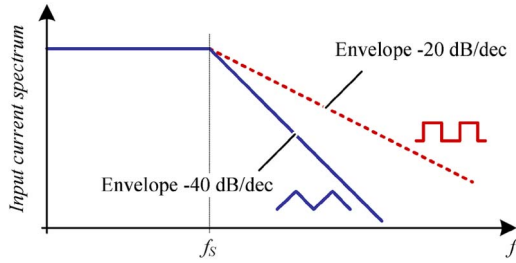


Fig. 3. Typical envelopes of the input current spectrum $I_{in}(f)$ of rectangular and triangular shapes.

f_D can be found directly to $f_D = f_s$ for switching frequencies higher than 150 kHz and to $f_D = n \cdot f_s$ in case of n parallel (interleaved) converter stages. However, for design frequencies below 150 kHz, not the first appearing peak but the m th multiple appearing first beyond 150 kHz [cf. Fig. 2(c)] is relevant for the input filter design. Therefore, the design frequency is then generally given by

$$f_D = m \cdot n \cdot f_s \quad (7)$$

with the factor m

$$m = \text{ceil} \left(\frac{150 \text{ kHz}}{n \cdot f_s} \right) \quad (8)$$

where the function ceil represents the round-up operation.

The estimated voltage peak in the frequency domain at f_D can now be calculated under consideration of the decay of the voltage peak height with increasing frequency (cf. Fig. 3)

$$U_{\text{est}}(f_D) [\text{dB}\mu\text{V}] = 20 \cdot \log \left(\frac{U_{\text{LISN}}}{m^a} \cdot \frac{1}{\mu\text{V}} \right) \quad (9)$$

with $a = 1$ for the case of a rectangular input current waveform and $a = 2$ for the case of a triangular input current shape.

Summing up, the introduced simplified estimation of the EMI filter requirements is given by the following:

- 1) simulating or calculating the total converter *rms* input current $I_{in,rms}$;
- 2) defining the design frequency f_D according to (7);
- 3) calculating $U_{\text{est}}(f_D)$ according to (9);
- 4) calculating the required filter attenuation by inserting $U_{\text{est}}(f_D)$ instead of $U_{QP}(f_D)$ in (1).

IV. FILTER VOLUME OPTIMIZATION

In the previous section, the DM filter requirements have been derived by a straightforward approximation. Out of these requirements, the goal of this section will be to design a DM filter, as shown in Fig. 1, with a minimal volume. It has to be stated that, in order to avoid filter resonances, an additional passive damping network can be applied [3], which is not done here for better illustration. The filter inductor volume is generally proportional to the stored energy and therefore given by

$$V_L \propto k_L \cdot L \cdot \hat{I}_{in}^2 \quad (10)$$

whereby k_L is a constant factor that describes the proportionality between the stored energy $E_L = 1/2 \cdot L \cdot I_{in}^2$ and the induc-

tor volume. This factor can be calculated from manufacturer's data for different inductor core dimensions, inductance values, and current ratings. However, for practical inductor designs with several cores from various manufacturers, it has been found that linear terms dependent on the input current and the inductance value also appear in the volume function. Thus, an approximation according to [13]

$$V_L = k_{L1} \cdot L \cdot \hat{I}_{in}^2 + k_{L2} \cdot L + k_{L3} \cdot \hat{I}_{in} \quad (11)$$

can be defined. The resulting inductor boxed-volume curves in dependence on the inductance value and the current is shown in Fig. 4(a) along with the specific volumetric values k_{L1} , k_{L2} , and k_{L3} . Here, only toroid cores from [18] have been considered due to their highest volume/inductance ratio [16].

The capacitor volume, on the other hand, scales with the stored energy plus a constant offset factor, which is also dependent on the voltage [13]

$$V_C = k_{C1} \cdot C \cdot \hat{U}_{in}^2 + k_{C2}(\hat{U}_{in}) \quad (12)$$

whereby the factor k_{C1} describes the proportionality of the capacitor volume and the stored energy and k_{C2} is a voltage-dependent factor. These factors can be derived analogously to k_{L1} , k_{L2} , and k_{L3} from manufacturer's data. In Fig. 4(b), the volume function (again for boxed volumes) is shown for a selection of available filter capacitors with 275-V *rms* rating together with the constant factors k_{C1} and k_{C2} .

As a result, a volume optimization of the DM filter volume utilizing the constant factors k_{L1} , k_{L2} , k_{L3} , k_{C1} , and k_{C2} can be done by minimizing the filter volume function [13]

$$V_{\text{tot}} = n_f \cdot (2 \cdot V_L + V_C) \rightarrow \min \quad (13)$$

whereby (2) must be fulfilled.

Solving (11)–(13) with (2) leads to the optimum filter component parameters for a certain number of filter stages n_f and a specific required attenuation Att_{req} (as calculated in Section III) at the design frequency f_D

$$C = \sqrt{\frac{(k_{L1} \cdot \hat{I}_{in}^2 + k_{L2}) \cdot n_f \sqrt{Att_{\text{req,DM}}}}{2 \cdot k_{C1} \cdot \hat{U}_{in}^2 \cdot (2\pi \cdot f_D)^2}} \quad (14)$$

$$L = \sqrt{\frac{k_{C1} \cdot \hat{U}_{in}^2 \cdot n_f \sqrt{Att_{\text{req,DM}}}}{2 \cdot (k_{L1} \cdot \hat{I}_{in}^2 + k_{L2}) \cdot (2\pi \cdot f_D)^2}} \quad (15)$$

The total DM filter volume can finally be found to be

$$V_{\text{tot}} = n_f \cdot k_{C2} + 2n_f \cdot k_{L3} \cdot \hat{I}_{in} + 3n_f \cdot \sqrt{\frac{(k_{L1} \cdot \hat{I}_{in}^2 + k_{L2}) \cdot (k_{C1} \cdot \hat{U}_{in}^2) \cdot n_f \sqrt{Att_{\text{req,DM}}}}{2(2\pi \cdot f_D)^2}} \quad (16)$$

and is dependent on the volumetric constant factors, the input current and voltage (or the input power, respectively), the required attenuation Att_{req} , and the number of filter stages n_f .

Looking at (16), one can see that the filter volume is also depending on the number of filter stages n_f . However, which

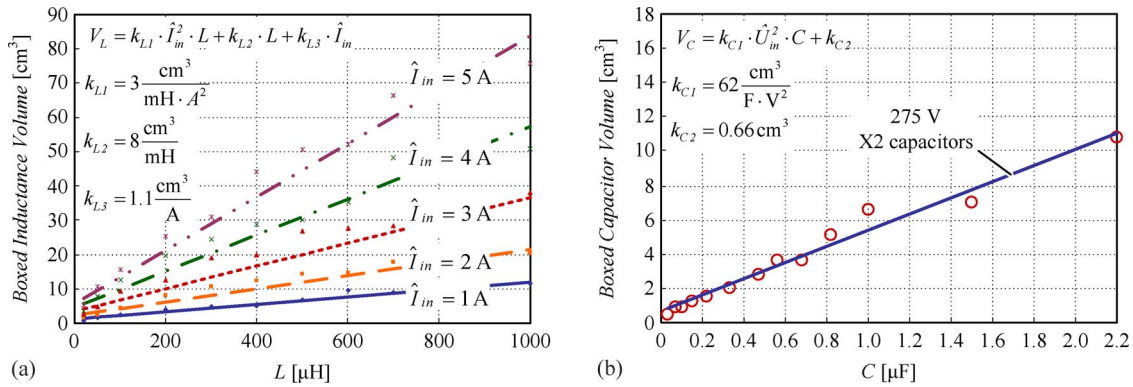


Fig. 4. (a) Inductor boxed-volume approximation for DM filter inductances using *Magnetics* toroid cores [18] in dependence on the inductance value. (b) Volume approximation for DM filter capacitors with 275-V *rms* rating in dependence on the capacitance value.

number of filter stages will lead to a minimum volume filter? To answer this, a differentiation of (16) with respect to n_f , equalizing with zero and solving by n_f , would deliver a solution. However, since the n_f th root of the required attenuation Att_{req} is part of (16), an analytical solution is associated with a very high mathematical effort. Therefore, a graphical solution will be presented subsequently.

Fig. 5 shows the resulting DM filter volume curves for different input power P_{in} and design frequency f_D combinations in dependence on the required attenuation Att_{req} and the number of filter stages n_f .

One can see that the resulting filter volume strongly depends on the input power P_{in} and the required attenuation Att_{req} , whereas the optimum number of filter stages is almost independent on P_{in} . For higher power levels, similar results can be drawn, which are not shown here for the sake of brevity. However, since power converters for higher power levels are typically driven with three phases, a three-phase EMI filter would also be necessary. The shown optimizations can be carried out for such filters in an analogous manner.

Concerning the design frequency f_D , it can be seen in Fig. 5 that the filter volume as well as the optimum number of filter stages are depending on f_D . As mentioned in the previous section, the design frequency f_D means the first multiple of the switching frequency f_S within the measurement range of 150 kHz–30 MHz. This leads to the fact that two converters with $f_S = 100$ kHz and $f_S = 200$ kHz will have the same design frequency. However, the resulting required attenuation Att_{req} will show a lower value for the converter with $f_S = 100$ kHz, since the amplitude of the noise peak is decreasing with 40 dB/dec (if the inductor current ripple values are chosen equally) and only the second harmonic falls within the EMI measurement range.

For the case of multiple parallel boost PFC cells (cf. Fig. 6), a converter with just one boost cell and $f_S = 200$ kHz will lead to the same design frequency f_D as a converter with two parallel boost cells and a switching frequency of $f_S = 100$ kHz. Here, the second one will lead to a lower required attenuation compared with the first one (if the inductor current ripple are again chosen equally), since the total input current ripple and, therefore, the required attenuation are reduced by interleaving.

V. DESIGN EXAMPLES

A. Example I: Analytical Calculation of $I_{noise,rms}$ for a Boost PFC Driven in Single CCM Operation

This section deals with the calculation of the appearing noise current $I_{noise,rms}$ exemplarily for a standard boost topology as shown in Fig. 6 but with only one boost cell. To ensure PFC, the inductor current is controlled in continuous conduction mode (CCM) [19]–[23].

The exemplary input current waveform with average current control [22], [23] can be seen in Fig. 7. To keep the focus on the essentials, the detailed calculations are given in Appendix A, and only the solution is presented here. The global noise *rms* current is given then with (28) by

$$I_{noise,CCM,rms}^2 = \frac{-64 \cdot \alpha + 12\pi + 9 \cdot \alpha^2 \pi}{18\pi} \cdot \alpha^2 \cdot \Delta I_{L,CCM,max}^2 \quad (17)$$

with the voltage ratio $\alpha = \hat{U}_{in}/U_0$ and the chosen maximum inductance current ripple $\Delta I_{L,CCM,max}$. With this, the required attenuation, which has to be provided by the EMI filter, can be found by inserting (17) into (6), (9), and (1).

In Table II, the resulting estimated noise voltages U_{est} and calculated QP noise voltages U_{QP} , found by circuit simulations and calculations according to the steps mentioned in Section I for verification, for a boost converter with one boost stage driven in CCM and a rated input power of $P_{in} = 300$ W for different switching frequencies f_S are summarized. One can see that the estimated noise voltage U_{est} only differs in the range of a few decibels in comparison with the exactly calculated QP noise voltage U_{QP} .

Additionally, the optimum number of filter stages $n_{f,opt}$ and the resulting filter components together with the estimated filter volume V_{tot} are summarized in Table II. Interestingly, for high switching frequencies, an EMI filter with only one filter stage leads to a minimum volume design, whereas in all other cases, a filter with two stages will be preferably concerning a minimal volume.

B. Example II: Estimation of $I_{noise,rms}$ by Circuit Simulations for a Boost PFC Driven in Dual Interleaved DCM Operation

For topologies with a complicated or even unknown input current waveform, it is recommended to derive the resulting

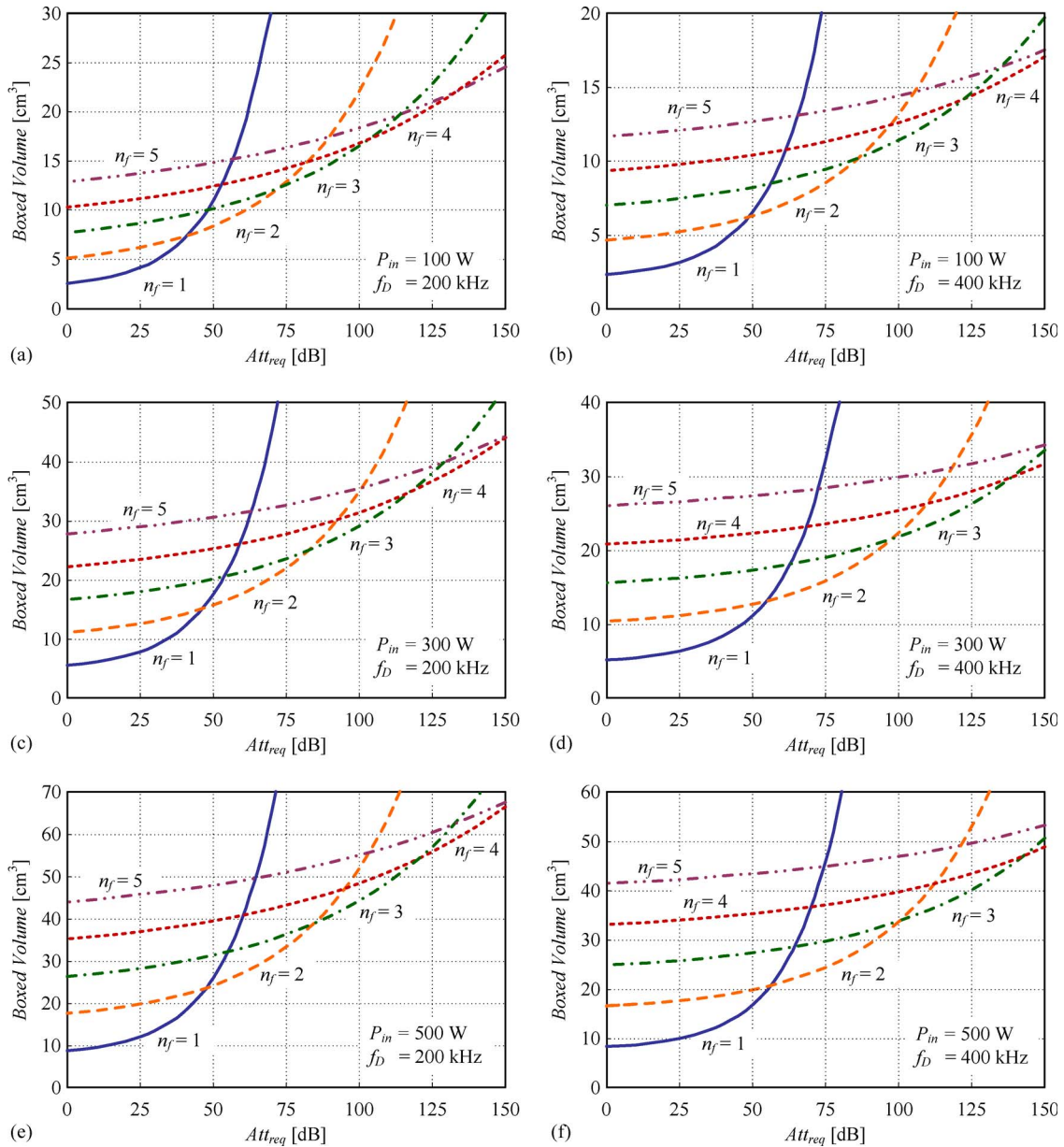


Fig. 5. Boxed-volume curves of the DM filter for a single-phase power converter in dependence on the required attenuation Att_{req} , the input power P_{in} , and the number of filter stages n_f for a 275-V rms rating.

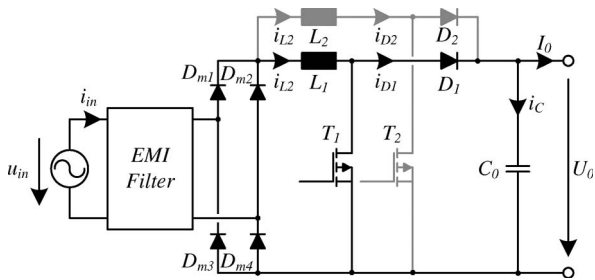


Fig. 6. Topology of a boost converter with n parallel (interleaved) boost cells.

input current rms value by numerical circuit simulations. One exemplary topology with a complicated input current is shown in Fig. 6 with two or more (n) parallel (interleaved) boost cells driven in discontinuous conduction mode (DCM) [24].

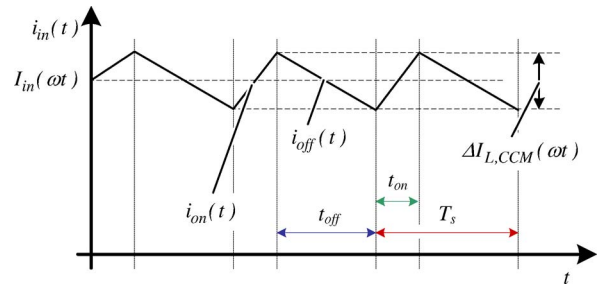


Fig. 7. Exemplary input current waveform for a boost converter with one boost stage driven in CCM.

In the case of $n = 2$, the total input current value $I_{in,rms}$ can be found by circuit simulations and used to calculate the noise rms current value $I_{noise,rms}$ out of (4) and (5) with the known rated input power P_{in} . Again, this current leads, together with

TABLE II
ESTIMATED PEAK AND CALCULATED QP NOISE VOLTAGE SPECTRUM VALUES IN DEPENDENCE ON THE CONVERTER SWITCHING FREQUENCY f_s FOR A BOOST PFC ON SINGLE CCM OPERATION FOR CONSTANT BOOST INDUCTANCE VALUES FOR ALL SWITCHING FREQUENCIES. FOR THE CALCULATION OF THE REQUIRED ATTENUATION Att_{req} AND THE FILTER COMPONENT VALUES, A SAFETY MARGIN OF 6 dB WAS TAKEN INTO ACCOUNT BY EVALUATING (1)

Boost PFC in Single CCM Operation										
f_s [kHz]	f_D [kHz]	U_{QP} [dB μ V]	U_{est} [dB μ V]	Error [dB]	Att_{req} [dB]	$n_{f,opt}$	V_{tot} [cm ³]	C [nF]	L [μ H]	
75	150	135.0	137.5	2.5	65.5	2	22.2	214	114	
100	200	133.8	135.0	1.2	63.0	2	18.4	150	80	
200	200	139.0	141.0	2.0	69.0	2	20.1	178	95	
400	300	135.0	135.0	0.0	63.0	2	14.4	75	40	

TABLE III
ESTIMATED PEAK AND CALCULATED QP NOISE VOLTAGE SPECTRUM VALUES IN DEPENDENCE ON THE CONVERTER SWITCHING FREQUENCY f_s FOR A BOOST PFC IN DUAL DCM OPERATION. FOR THE CALCULATION OF THE REQUIRED ATTENUATION Att_{req} AND THE FILTER COMPONENT VALUES, A SAFETY MARGIN OF 6 dB WAS TAKEN INTO ACCOUNT BY EVALUATING (1)

Boost PFC in Dual DCM Operation										
f_s [kHz]	f_D [kHz]	U_{QP} [dB μ V]	U_{est} [dB μ V]	Error [dB]	Att_{req} [dB]	$n_{f,opt}$	V_{tot} [cm ³]	C [nF]	L [μ H]	
50	200	132.6	137.0	4.4	65.0	2	18.9	160	84	
100	200	145.7	149.0	3.3	77.0	2	22.7	224	120	
200	400	147.0	149.9	2.9	77.9	2	16.4	115	61	
400	800	147.5	151.3	3.8	84.3	2	13.7	69	37	

(6), (9), and (1), to the required attenuation Att_{req} at the design frequency f_D according to (7). As in the previous section, the expected noise voltage U_{est} in dependence on the switching frequency for a PFC boost converter with two parallelized boost cells driven in DCM and a rated input power of $P_{in} = 300$ W has been calculated and is summarized in Table III. For reasons of comparison, the exactly calculated QP noise voltage U_{QP} is also shown in Table III.

One can see that the estimated and calculated noise voltages only differ in the range of 3–6 dB (cf. Table III), which represents a sufficient accuracy. In all cases, a positive error is obtained, which means a slight overdimensioning of the filter.

Again, the resulting optimum number of filter stages $n_{f,opt}$, together with the filter component values and the total filter volume, has been calculated according to (14)–(16) and is compiled in Table III. An interesting result is that, for DCM operation and the chosen power range, two filter stages are always preferable concerning a minimum volume design. Compared with single CCM operation, the resulting filter volume is in the same range for equal switching frequencies and shows decreasing behavior for increasing switching frequencies. As a matter of fact, reduced EMI filter requirements can be achieved by interleaving. This is particularly interesting for DCM operation, where the inductor current ripple is higher than for CCM operation.

VI. EXPERIMENTAL VERIFICATION

For the verification of the previously done examinations, a laboratory setup of the boost converter, as shown in Fig. 6, with two parallel boost cells driven in DCM operation, a switching frequency of $f_s = 200$ kHz (resulting in a design frequency of $f_D = 400$ kHz), and a rated input power of $P_{in} = 300$ W has been built up. Since the noise-emission limit for industrial

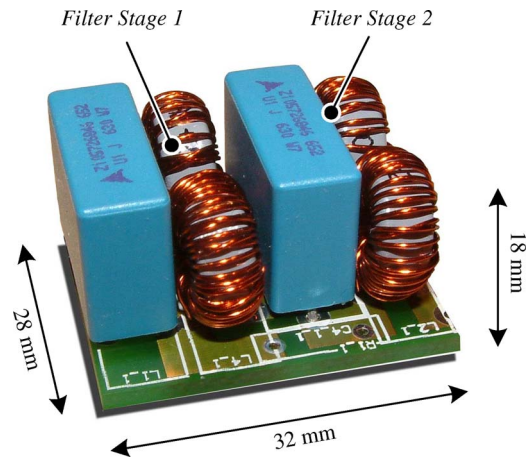


Fig. 8. DM EMI filter for the laboratory boost converter setup with two parallel boost cells, a switching frequency $f_s = 200$ kHz, and a rated output power $P_0 = 300$ W.

equipment (class A) is given by $Limit(400 \text{ kHz}) = 78 \text{ dB} \cdot \mu\text{V}$ according to [2], the required attenuation for this setup can be found with the estimated value in Table III and an additional margin of 6 dB according to (1) as $Att_{req} = 149.9 \text{ dB} \cdot \mu\text{V} - 78 \text{ dB} \cdot \mu\text{V} + 6 \text{ dB} = 77.9 \text{ dB}$. This leads to an optimum number of filter stages $n_f = 2$ [cf. Fig. 5(d)]. According to (14)–(16) and as given in Table III, the filter component values can be found as $L_1 = L_2 = L = 61 \mu\text{H}$ and $C_1 = C_2 = C = 115 \text{ nF}$. This results in a theoretical total boxed filter volume of approximately 16.4 cm^3 . The EMI filter of the laboratory setup is shown in Fig. 8, and the real volume can be calculated, according to the dimensions shown in Fig. 8, as 16.1 cm^3 , which also confirms the parametric model as shown in Fig. 4.

Conducted EMI measurement results done with this laboratory setup with and without the designed DM filter are shown in

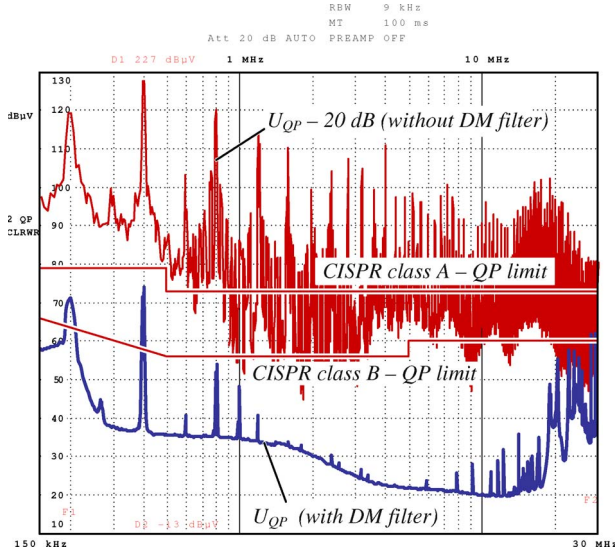


Fig. 9. EMI measurements done with a laboratory boost converter setup with two parallel boost cells, a switching frequency $f_s = 200$ kHz, and a rated output power $P_0 = 300$ W. For both measurements, a sufficiently large common-mode filter has been employed in order to verify only the proposed DM filter design approach. For the measurement without the DM filter, a 20-dB attenuator was used in order to not exceed the measurement range.

Fig. 9. Hereby, a sufficiently large common-mode filter, which is not shown in Fig. 8, has been employed additionally in order to verify only the proposed DM filter design guideline. For the measurement without the input filter, the measured signal had to be attenuated by an external 20-dB attenuator in order to keep the signal within the measurement range. One can see the highest appearing peak at 400 kHz, which represents twice the switching frequency f_s , due to two parallel boost cells [cf. f_D in Table III and (7)]. This peak shows a magnitude of approximately $148 \text{ dB} \cdot \mu\text{V}$, which matches well with the estimated value [$149.9 \text{ dB} \cdot \mu\text{V}$ (see Table III)]. As for the curve with DM filter in Fig. 9, one can see that the implemented EMI filter is sufficient to fully comply with the Comite Internationale Special des Perturbations Radioelectrotechnique (CISPR) Class A standards in the whole measurement range. The first appearing peak still has a resulting margin to the class A noise-emission limit of approximately 5 dB, which is due to the included safety margin.

The realized laboratory setup was designed for industrial usage, wherefore the CISPR Class A limits (cf. Fig. 9) had to be fulfilled and were inserted in (1). In order to comply with the CISPR Class B limit for commercial applications, the same design routine can be used by using the Class B limits for (1).

VII. CONCLUSION

In this paper, a straightforward guideline for a simplified DM EMI input filter design has been given. In a first step, the filter requirements are estimated out of the converter input *rms* current by using only a few simple equations. Furthermore, a law to calculate the design frequency, which is needed for the input filter design, is introduced.

In a second step, a volume optimization of the DM EMI filter based on volumetric parameters of the filter inductances and ca-

pacitors is given. The resulting filter volume mainly depends on the previously found attenuation Att_{req} , the design frequency f_D , the delivered power P_{in} , and finally, the number of filter stages n_f . It has been shown that an optimum number of filter stages in dependence on the previously mentioned parameters exists. This optimum number of filter stages has been evaluated exemplarily for different power levels (100, 300, and 500 W) and design frequencies (200 and 400 kHz) in dependence on the required attenuation in the range of 0–150 dB.

Two examples, where the total *rms* converter input currents have been calculated and simulated, prove the done examinations. The occurring error between the estimated noise voltage and the real QP noise voltage lies only in the range of a few decibels. Finally, experimentally conducted EMI measurements done with a laboratory setup of a PFC driven in dual DCM operation with a rated input power of $P_{in} = 300$ W and a switching frequency of $f_s = 200$ kHz prove the correctness of the introduced guideline.

Summing up, with the guideline presented in this paper, a fast and simple design of a DM EMI filter is possible, providing the required filter component values and the resulting filter volume.

APPENDIX

DETAILED ANALYTICAL CALCULATION OF $I_{noise,rms}$ FOR A BOOST PFC DRIVEN IN SINGLE CCM OPERATION

The turn-on t_{on} and turn-off t_{off} times of the switch T_1 in Fig. 6 to ensure the continuous current behavior are generally given by

$$t_{on}(\omega t) = \frac{1}{f_s} \cdot (1 - \alpha \sin(\omega t)) \quad (18)$$

$$t_{off}(\omega t) = \frac{1}{f_s} \cdot \alpha \sin(\omega t) \quad (19)$$

respectively, with the switching frequency $f_s = 1/T_s$ and the voltage ratio $\alpha = \hat{U}_{in}/U_0$. The appearing current ripple $\Delta I_{L,CCM}(\omega t)$ (cf. Fig. 7) is generally defined by the inductance law

$$\Delta I_{L,CCM}(\omega t) = \hat{U}_{in}(\omega t) \cdot \frac{t_{on}(\omega t)}{L_{CCM}} \quad (20)$$

with the boost inductance for CCM

$$L_{CCM} = \frac{U_0}{4 \cdot f_s \cdot \Delta I_{L,CCM,max}} \quad (21)$$

and the chosen maximum inductor current ripple $\Delta I_{L,CCM,max}$. For the subsequent calculation of the global input *rms* current, the current decays during the on-time ($i_{on}(t)$) and off-time ($i_{off}(t)$) have to be known. These currents can be assumed to be linear functions

$$i_{on}(t) = \frac{\Delta I_{L,CCM}(\omega t)}{t_{on}(\omega t)} \cdot t + I_{in}(\omega t) - \frac{\Delta I_{L,CCM}(\omega t)}{2} \quad (22)$$

$$i_{off}(t) = -\frac{\Delta I_{L,CCM}(\omega t)}{t_{off}(\omega t)} \cdot t + I_{in}(\omega t) + \frac{\Delta I_{L,CCM}(\omega t)}{2} \quad (23)$$

respectively.

For the derivation of the global *rms* current I_{rms} , first, the local *rms* current i_{rms} of one switching cycle has to be calculated, since the switching frequency is much higher than the mains frequency

$$i_{\text{rms}}^2 = \frac{1}{T_S} \int_{T_S} i(t)^2 dt. \quad (24)$$

Integrating the local *rms* current i_{rms}^2 out of (24) over one mains period leads to the global *rms* current

$$I_{\text{rms}}^2 = \frac{1}{2\pi} \int_{-\pi}^{\pi} i_{\text{rms}}^2(\omega t) d\omega t. \quad (25)$$

Inserting the before mentioned on- and off-currents in (24) leads to the local *rms* input current

$$i_{\text{in,CCM,rms}}^2(\omega t) = \frac{1}{T_S} \cdot \left(\int_0^{t_{\text{on}}} i_{\text{on}}^2(t) dt + \int_0^{t_{\text{off}}} i_{\text{off}}^2(t) dt \right) \quad (26)$$

and, furthermore, by solving the integral as

$$i_{\text{in,CCM,rms}}^2(\omega t) = \underbrace{\hat{i}_{\text{in}}^2(\omega t)}_{\text{Part 1}} + \underbrace{\frac{\Delta I_{L,\text{CCM}}^2(\omega t)}{12}}_{\text{Part 2}}. \quad (27)$$

Looking at (27), one can see that this current consists of two parts, namely, the input current I_{in} (*Part 1*), and the current ripple $\Delta I_{L,\text{CCM}}(\omega t)$ (*Part 2*), which represents the noise current (cf. Section III). Integrating *Part 2* over a half mains period with (18), (20), and (21) finally leads to the global *rms* noise current

$$I_{\text{noise,CCM,rms}}^2 = \frac{-64 \cdot \alpha + 12\pi + 9 \cdot \alpha^2 \pi}{18\pi} \cdot \alpha^2 \cdot \Delta I_{L,\text{CCM,max}}^2. \quad (28)$$

REFERENCES

- [1] *Electromagnetic Compatibility (EMC) Part 3-2: Limits—Limits for Harmonic Current Emissions (Equipment Input Current ≤ 16 A per Phase)*, I. I. E. Commission, Geneva, Switzerland, 2001. Consol. Ed. 2.1.
- [2] *Information Technology Equipment—Radio Disturbance Characteristics—Limits and Methods of Measurement—Publication 22*, C.I.S.P.R., Geneva, Switzerland, 1997.
- [3] T. Nussbaumer, M. L. Heldwein, and J. W. Kolar, "Differential mode input filter design for a three-phase buck-type PWM rectifier based on modeling of the EMC test receiver," *IEEE Trans. Ind. Electron.*, vol. 53, no. 5, pp. 1649–1661, Oct. 2006.
- [4] M. Albach, "Conducted interference voltage of AC–DC converters," in *Proc. 17th Annu. IEEE Power Electron. Spec. Conf.*, 1986, pp. 230–212.
- [5] J. C. Salmon, "Techniques for minimizing the input current distortion of current-controlled single-phase boost rectifiers," *IEEE Trans. Power Electron.*, vol. 8, no. 4, pp. 509–520, Oct. 1993.
- [6] J. Wang, W. Dunford, and K. Mauch, "A comparison of modified boost converters with continuous inductor current mode and ripple free input current with conventional converters," in *Conf. Rec. 31st IEEE IAS Annu. Meeting*, Oct. 6–10, 1996, vol. 2, pp. 878–885.
- [7] J. Wang, W. G. Dunford, and K. Mauch, "Analysis of a ripple-free input-current boost converter with discontinuous conduction characteristics," *IEEE Trans. Power Electron.*, vol. 12, no. 4, pp. 684–694, Jul. 1997.
- [8] V. Grigore, J. Kyrya, and J. Rajamaki, "Input filter design for power factor correction converters operating in discontinuous conduction mode," in *Proc. IEEE Int. Symp. Electromagn. Compat.*, Aug. 2–6, 1999, vol. 1, pp. 145–150.
- [9] L. Rosetto, S. Buso, and G. Spiazzi, "Conducted EMI issues in a 600-W single-phase boost PFC design," *IEEE Trans. Ind. Appl.*, vol. 36, no. 2, pp. 578–585, Mar./Apr. 2000.
- [10] S. Chandrasekaran, S.A. Ragon, D. K. Lindner, Z. Gurdal, and D. Boroyevich, "Optimization of an aircraft power distribution subsystem," *J. Aircr.*, vol. 40, no. 1, pp. 16–26, 2003.
- [11] F. Barruel, J. Schanen, and N. Retiere, "Volumetric optimization of passive filter for power electronics input stage in the more electrical aircraft," in *Proc. 35th Annu. IEEE PESC*, Jun. 20–25, 2004, vol. 1, pp. 433–438.
- [12] W. Shen, F. Wang, D. Boroyevich, V. Stefanovic, and M. Arpilliere, "Optimizing EMI filter design for motor drives considering filter component high-frequency characteristics and noise source impedance," in *Proc. IEEE APEC*, 2004, pp. 669–674.
- [13] K. Raggl, T. Nussbaumer, and J. Kolar, "Model based optimization of EMC input filters," in *Proc. 11th Workshop COMPEL*, Aug. 17–20, 2008, pp. 1–6.
- [14] H.-I. Hsieh, J.-S. Li, and D. Chen, "Effects of X capacitors on EMI filter effectiveness," *IEEE Trans. Ind. Electron.*, vol. 55, no. 2, pp. 949–955, Feb. 2008.
- [15] S. Wang, J. van Wyk, and F. Lee, "Effects of interactions between filter parasitics and power interconnects on EMI filter performance," *IEEE Trans. Ind. Electron.*, vol. 54, no. 6, pp. 3344–3352, Dec. 2007.
- [16] M. L. Heldwein and J. W. Kolar, "Design of minimum volume EMC input filters for an ultra compact three-phase PWM rectifier," in *Proc. 9th COBEP*, Sep. 30–Oct. 4, 2007. [CD-ROM].
- [17] *Specification for Radio Disturbance and Immunity Measuring Apparatus and Methods Part II: Methods of Measurement of Disturbances and Immunity—Publication 16*, C.I.S.P.R., Geneva, Switzerland, 1999.
- [18] *Powder Cores Catalog*, Magnetics, Pittsburgh, 2005/2006.
- [19] S. Busquets-Monge, G. Soremekun, E. Hertz, C. Crebier, S. Ragon, J. Zhang, D. Boroyevich, Z. Gurdal, D. Lindner, and M. Arpilliere, "Design optimization of a boost power factor correction converter using genetic algorithms," in *Proc. 17th Annu. IEEE APEC*, Mar. 10–14, 2002, vol. 2, pp. 1177–1182.
- [20] S. Yip, H. Chung, and S. Hui, "A unified control scheme for a bidirectional AC–DC converter with high power quality," in *Proc. 16th Annu. IEEE APEC*, Mar. 4–8, 2001, vol. 1, pp. 74–80.
- [21] C. Zhou and M. M. Jovanovic, "Design trade-offs in continuous current-mode controlled boost power-factor correction circuits," in *Proc. HFPC*, 1992, pp. 209–219.
- [22] L. Rossetto, G. Spiazzi, and P. Tenti, "Control techniques for power factor correction converters," in *Proc. Int. Conf. Power Electron. Motion Control*, Warsaw, Poland, 1994, pp. 1310–1318.
- [23] E. Figueres, J. M. Benavent, G. Garcera, and M. Pascual, "A control circuit with load-current injection for single-phase power-factor-correction rectifiers," *IEEE Trans. Ind. Electron.*, vol. 54, no. 3, pp. 1272–1281, Jun. 2007.
- [24] K. Raggl, T. Nussbaumer, G. Doerig, J. Biela, and J. W. Kolar, "Comprehensive design and optimization of a high-power-density single-phase boost PFC," *IEEE Trans. Ind. Electron.*, vol. 56, no. 7, pp. 2574–2587, Jul. 2009.



Klaus Raggl (S'05) was born in Zams, Austria, in 1980. He received the M.S. degree in mechatronics from the Johannes Kepler University Linz, Linz, Austria, in 2005, and the Ph.D. degree from the Power Electronic Systems Laboratory (PES), Swiss Federal Institute of Technology (ETH) Zurich, Zurich, Switzerland, in 2009, where he worked on bearingless pump systems with high power density in the drive technology and magnetic bearings section.

Since April 2009, he has been with Hilti AG, Schaan, Liechtenstein, where he is working on high-performance drilling and demolition machines.



Thomas Nussbaumer (S'02–M'06) was born in Vienna, Austria, in 1975. He received the M.Sc. degree (with honors) in electrical engineering from the University of Technology Vienna, Vienna, Austria, in 2001, and the Ph.D. degree from the Power Electronic Systems (PES) Laboratory, Swiss Federal Institute of Technology (ETH) Zurich, Zurich, Switzerland, in 2004.

From 2001 to 2006, he was with the PES, where he conducted research on modeling, design, and control of three-phase rectifiers, power factor correction techniques, and electromagnetic compatibility. Since 2006, he has been with Levitronix GmbH, Zurich, Switzerland, where he is currently working on bearingless motors, magnetic levitation, and permanent-magnet motor drives for the semiconductor and biotechnology industry. His current research is focused on compact and high-performance mechatronic systems including novel power electronics topologies, control techniques, drive systems, sensor technologies, electromagnetic interference (EMI), and thermal aspects.



Johann W. Kolar (M'89–SM'04) received the Ph.D. degree (*summa cum laude/promotio sub auspiciis praesidentis rei publicae*) from the University of Technology Vienna, Vienna, Austria.

Since 1984, he has been working as an independent international consultant in close collaboration with the University of Technology Vienna, in the fields of power electronics, industrial electronics, and high performance drives. He has proposed numerous novel pulsewidth-modulation converter topologies, and modulation and control concepts, e.g., the Vienna Rectifier and the three-phase ac–ac sparse matrix converter. He has published over 250 scientific papers in international journals and conference proceedings and has filed more than 70 patents. He is currently with the Swiss Federal Institute of Technology, (ETH) Zurich, Zurich, Switzerland, where he was appointed Professor and Head of the Power Electronic Systems Laboratory, on February 1, 2001. The focus of his current research is on ac–ac and ac–dc converter topologies with low effects on the mains, e.g., for power supply of telecommunication systems, More-Electric Aircraft, and distributed power systems in connection with fuel cells. Further main areas of research are the realization of ultracompact intelligent-converter modules employing the latest power semiconductor technology (SiC), novel concepts for cooling, and electromagnetic-interference filtering, multidomain/multiscale modeling and simulation, pulsed power, bearingless motors, and Power microelectromechanical systems.

Dr. Kolar is a member of the Institute of Electrical Engineering in Japan (IEEJ) and of technical program committees of numerous international conferences in the field (e.g., Director of the Power Quality Branch of the International Conference on Power Conversion and Intelligent Motion). From 1997 through 2000, he served as an Associate Editor of the IEEE TRANSACTIONS ON INDUSTRIAL ELECTRONICS, and, since 2001, has served as an Associate Editor of the IEEE TRANSACTIONS ON POWER ELECTRONICS. Since 2002, he has also been an Associate Editor of the *Journal of Power Electronics* of the Korean Institute of Power Electronics and a member of the Editorial Advisory Board of the *IEEJ Transactions on Electrical and Electronic Engineering*. He is the recipient of the Best Transactions Paper Award of the IEEE Industrial Electronics Society in 2005. He was also the recipient of an Erskine Fellowship from the University of Canterbury, New Zealand, in 2003. In 2006, the European Power Supplies Manufacturers Association recognized the Power Electronics Systems Laboratory of ETH Zurich as the leading academic research institution in Europe.